

Low-Cost Exoskeletons for Learning Whole-Arm Manipulation in the Wild

Hongjie Fang^{*,1,3}, Hao-Shu Fang^{*,1}, Yiming Wang^{*,2},
Jiejie Ren², Jingjing Chen¹, Ruo Zhang¹, Weiming Wang², Cewu Lu^{1,3}
(* Equal contribution)

Abstract—While humans can use parts of their arms other than the hands for manipulations like gathering and supporting, whether robots can effectively learn and perform the same type of operations remains relatively unexplored. As these manipulations require joint-level control to regulate the complete poses of the robots, we develop *AirExo*, a low-cost, adaptable, and portable dual-arm exoskeleton, for teleoperation and demonstration collection. As collecting teleoperated data is expensive and time-consuming, we further leverage *AirExo* to collect cheap in-the-wild demonstrations at scale. Under our in-the-wild learning framework, we show that with only 3 minutes of the teleoperated demonstrations, augmented by diverse and extensive in-the-wild data collected by *AirExo*, robots can learn a policy that is comparable to or even better than one learned from teleoperated demonstrations lasting over 20 minutes. Experiments demonstrate that our approach enables the model to learn a more general and robust policy across the various stages of the task, enhancing the success rates in task completion even with the presence of disturbances. Project website: airexo.github.io.

I. INTRODUCTION

Robotic manipulation has emerged as a crucial field within the robot learning community and attracted significant attention from researchers. With the steady advancement of technologies such as deep learning, robotic manipulation has evolved beyond conventional grasping [9, 32] and pick-and-place tasks [31, 42], encompassing a diverse array of complex and intricate operations [2, 3, 6, 10].

Most of the current robotic manipulation research focuses on interacting with the environment solely with the end-effectors of the robots, which correspond to the hands of human beings. However, as humans, we can also use other parts of our arms to accomplish or assist with various tasks in daily life. For example, holding objects with lower arms, closing fridge door with elbow, *etc.* In this paper, we aim to investigate and explore the ability of robots to effectively execute such tasks. To distinguish from the classical manipulation involving end-effectors, we refer to these actions as **whole-arm manipulation**. Since most whole-arm manipulation tasks require the coordinated collaboration of both limbs, we formalize them into the framework of the bimanual manipulation problem.

¹ School of Electronic Information and Electrical Engineering, Shanghai Jiao Tong University.

² School of Mechanical Engineering, Shanghai Jiao Tong University.

³ Shanghai Artificial Intelligence Laboratory.

email: galaxies@sjtu.edu.cn, fhaoshu@gmail.com, sommerfeld, jiejiiren, jjchen20, wangweiming, lucewu@sjtu.edu.cn, ruozhang0608@gmail.com.

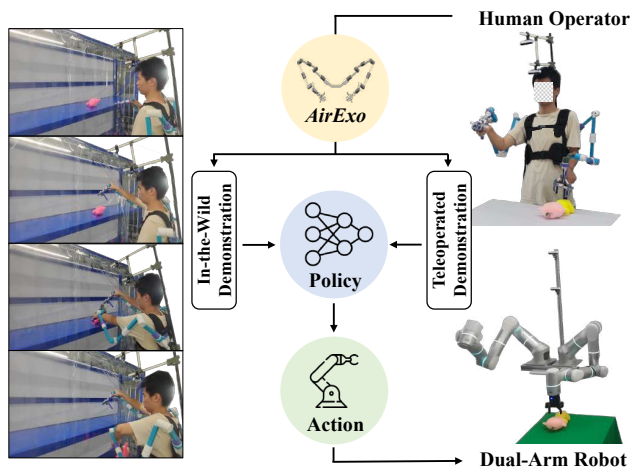


Fig. 1: The methodology of our in-the-wild learning framework with low-cost exoskeletons *AirExo*. It empowers the human operator to not only control the dual-arm robots for collecting teleoperated demonstrations but also directly record in-the-wild demonstrations. Besides commonly-used teleoperated demonstrations, our proposed learning framework also leverages the extensive and cheap in-the-wild demonstrations in policy learning, resulting in a more general and robust policy compared to training with even more teleoperated demonstrations.

While whole-arm manipulation is natural and simple for humans, it can become challenging for robots. First, whole-arm manipulation usually implies extensive contact with the surrounding environment and collision risks during manipulation. Second, whole-arm manipulation necessitates precise movement of the entire robot pose, as opposed to the conventional methods of only reaching the end-effector pose at the destination. An intuitive approach to address these two challenges is to adapt joint-level control for robots. To enable that, we adopt a joint-level imitation learning schema, wherein joint-level control is needed when collecting the robot demonstration.

Recently, Zhao *et al.* [45] introduced an open-source low-cost ALOHA system which exhibits the capability to perform joint-level imitation learning through real-world teleoperated data. ALOHA system leverages two small, simple and modular bimanual robots ViperX [36] and WidowX [39] that are almost identical to each other, to establish a leader-follower framework for teleoperation. Due to the limited payload of the robots, they focus more on fine-grained manipulation.

Besides, their hardware cannot be seamlessly adapted to other robots commonly employed for laboratory research or industrial purposes. Similarly, while several literatures [8, 14, 16, 18, 44] also designed special exoskeletons for certain humanoid robots or robot arms, the cross-robot transferability of their exoskeletons remain a challenge.

To address the above issues, we develop *AirExo*, an *open-source, low-cost, robust and portable* dual-arm exoskeleton system that can be quickly modified for different robots. All structural components of *AirExo* are *universal* across robots and can be fabricated entirely through 3D printing, enabling easy assembly even for non-experts. After calibration with a dual-arm robot, *AirExo* can achieve precise joint-level teleoperations of the robot.

Contributed to its portable property, *AirExo* enables *in-the-wild data collection for dexterous manipulation without needing a robot*. Humans can wear the dual-arm exoskeleton system, conduct manipulation in the wild, and collect demonstrations at scale. This breakthrough capability not only simplifies data collection but also extends the reach of whole-arm manipulation into unstructured environments, where robots can learn and adapt from human interactions. The one-to-one mapping of joint configurations also reduces the barriers of transferring policies trained on human-collected data to robots. Experiments show that with our in-the-wild learning framework, the policy can become more sample efficient for the expensive teleoperated demonstrations, and can acquire more high-level knowledge for task execution, resulting in a more general and robust strategy. The source code, data and exoskeleton models are released at the [project website](#).

II. RELATED WORKS

A. Imitation Learning

Imitation learning has been widely applied in robot learning to teach robots how to perform various tasks by observing and imitating demonstrations from human experts. One of the simplest methods in imitation learning is behavioral cloning [26], which learns the policy directly in a supervised manner without considering intentions and outcomes. Most approaches parameterize the policy using neural networks [2, 5, 30, 43, 45], while non-parametric VINN [25] leverages the weighted k -nearest-neighbors algorithm based on the visual representations extracted by BYOL [13] to generate the action from the demonstration database. This simple but effective method can also be extended to other visual representations [21, 22, 24, 28] for robot learning.

In the context of imitation learning for bimanual manipulation, Xie *et al.* [40] introduced a paradigm to decouple the high-level planning model into the elemental movement primitives. Several literature have focused on designing special frameworks to solve specific tasks, such as knot tying [17, 33], banana peeling [16], culinary activities [20], and fabric folding [38]. Addressing the challenge of non-Markovian behavior observed in demonstrations, Zhao *et al.* [45] utilized the notion of action chunking as a strategy to enhance overall performance.

B. Teleoperation

Demonstration data play a significant role in robotic manipulation, particularly in the methods based on imitation learning. For the convenience of subsequent robot learning, these demonstration data are typically collected within the robot domain. A natural approach to gather such demonstrations is human teleoperation [23], where a human operator remotely controls the robot to execute various tasks.

Teleoperation methods can be broadly categorized into two classes based on their control objectives: one aimed at manipulating the end-effectors of the robots [2, 7, 10, 15, 29, 43] and one focused on regulating the complete poses of the entire robots, such as exoskeletons [8, 14, 16, 34, 44] and a pair of leader-follower robots [45]. For whole-arm manipulation tasks, we need to control the full pose of the robots, which makes exoskeletons a relatively favorable option under this circumstance.

C. Learning Manipulation in the Wild

Despite the aforementioned teleoperation methods allow us to collect robotic manipulation data, the robot system is usually expensive and not portable, posing challenges to collect demonstration data at scale. To address this issue, previous research has explored the feasibility of learning from interactive human demonstrations, *i.e.* in-the-wild learning for robotic manipulation [1, 4, 18, 27, 32, 41]. In contrast to the costly robot demonstrations, in-the-wild demonstrations are typically cheap and easy to obtain, allowing us to collect a large volume of such demonstrations conveniently.

Typically, there are two primary domain gaps for learning manipulation in the wild: (1) the gap between human-operated images and robot-operated images, and (2) the gap between human kinematics and robot kinematics. The former gap can be solved through several approaches: by utilizing specialized end-effectors that match the end-effectors of the robots [18, 41]; by initially pre-training with in-the-wild data and subsequently fine-tuning with robot data [32]; or by applying special image processing technique to generate agent-agnostic images [1]. The latter gap is currently addressed by applying structure from motion algorithms [32, 41], adopting a motion tracking system [27], or training a pose detector [1, 37] to extract the desired poses. However, these methods are not suitable for whole-arm dexterous manipulation, since motion tracking usually focuses on the end-effector, and pose detector is vulnerable to visual occlusions and does not map to the robot kinematics.

Thus, in this paper we develop a low-cost and portable exoskeleton to serve as a bridge between human motion and robot motion. It can be applied not only to the teleoperation of robots but also as a powerful tool for learning manipulation in the wild.

III. AIREXO: AN OPEN-SOURCE, PORTABLE, ADAPTABLE, INEXPENSIVE AND ROBUST EXOSKELETON

A. Exoskeleton

From the preceding discussions in Sec. I, we summarize the following 5 key design objectives of an exoskeleton: (1)

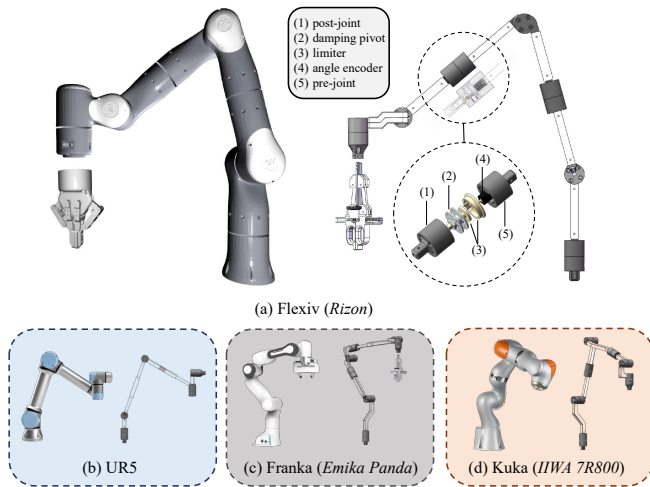


Fig. 2: *AirExo* models for different types of robots. Notice that the internal structure of the joints is standardized, only the linkages are altered to accommodate different robotic arm configurations.

affordability; (2) adaptability; (3) portability; (4) robustness and (5) maintenance simplicity. Based on these design objectives, we develop *AirExo* as follows.

In this paper, we employ two Flexiv Rizon arms [11] for experiments. As a result, the structural design of *AirExo* is predominantly tailored to their specifications. Meanwhile, to ensure its universality, it can be easily modified for use with other robotic arms like UR5 [35], Franka [12] and Kuka [19], as depicted in Fig. 2.

Based on the morphology of our robot system, *AirExo* is composed of two symmetrical arms, wherein the initial 7 degree-of-freedom (DoFs) of each arm correspond to the DoFs of the robotic arm, and the last DoF corresponds to the end-effector of the robotic arm. Here, we design a two-finger gripper with 1 DoF as an optional end-effector for each arm. Overall, *AirExo* is capable of simulating the kinematics of the robot across its entire workspace, as well as emulating the opening and closing actions of the end-effectors.

According to design objective (3), to improve the wearable experience for operators and concurrently enhance task execution efficiency, we dimension *AirExo* to be 80% of the robot’s size, based on the length of the human arm. In the end-effector of the exoskeleton, we design a handle and a scissor-like opening-closing mechanism to simulate the function of a two-fingered gripper, while also facilitating gripping actions by the operator. The two arms of the exoskeleton are affixed to a base, which is mounted on a vest. This allows the operator to wear it stably, and evenly distributing the weight of the exoskeleton across the back of the operator to reduce the load on the arms, thereby enabling more flexible arm motions. Additionally, an adjustable camera mount can be installed on the base for image data collection during operations.

The joints of *AirExo* adapt a dual-layer structure, with the outer case divided into two parts: the portion proximate to the base is referred to as the *pre-joint*, while the other half is called the *post-joint*. As illustrated in Fig. 2(a), these two components are connected via a metal *damping pivot*, and

their outer sides are directly linked to the connecting rod. *AirExo* primarily achieves high-precision and low-latency motion capture through the *angle encoders* (with a resolution of 0.08 degrees), whose bases are affixed to the *pre-joints*. The pivots of the encoders are connected to the *post-joint* through a *limiter*, which is comprised of a dual-layer disc and several steel balls to set the angle limit for each joint. The dual-layer joint structure ensures that the encoders remain unaffected by bending moments during motions, rotating synchronously with the joints, which safeguards the encoders and reduces failures effectively. This aligns with the design objective (4) and (5).

Except the fasteners, damping pivots, and electronic components, all other components of *AirExo* are fabricated using PLA plastic through 3D printing. The material has a high strength and a low density, thereby achieving a lightweight but robust exoskeleton. The prevalence of 3D-printed components allows the exoskeleton to be easily adapted to different robots. This adaptation entails adjusting the dimensions of certain components based on the target robot’s specifications and subsequently reprinting and installing them, without modifying the internal structure. *AirExo* costs approximately \$600 in total (16 encoders of \$30 each; 3D printing materials, mechanical parts and wires \$120), which is in accordance with the design objective (1).

For more details about *AirExo*, including models and the installation guide, please refer to our [project website](#).

B. Calibration and Teleoperation

Since *AirExo* shares the same morphology with the dual-arm robot except for the scale, the calibration process can be performed in a quite straightforward manner. After positioning the robot arms at a specific location like a fully extended position, and aligning the exoskeleton to match the robot posture, we can record the joint positions $\{q_i^{(c)}\}_{i=1}^d$ and the encoder readings $\{p_i^{(c)}\}_{i=1}^d$ of *AirExo*, where d denotes the DoFs. Consequently, during teleoperation, we only need to fetch the encoder readings $\{p_i\}_{i=1}^d$ and transform them into the corresponding joint positions $\{q_i\}_{i=1}^d$ using Eqn. (1), and let the robot moves to the desired joint positions:

$$q_i = \min \left(\max \left(q_i^{(c)} + k_i(p_i - p_i^{(c)}), q_i^{\min} \right), q_i^{\max} \right), \quad (1)$$

where $k_i \in \mathbb{R}$ is the coefficient controlling direction and scale, and q_i^{\min}, q_i^{\max} denote the joint angle limits of the robotic arms. Typically, we set $k = \pm 1$, representing the consistency between the encoder direction of the exoskeleton and the joint direction of the robot. For grippers, we can directly map the angle range of the encoders to the opening and closing range of the grippers for teleoperation.

After calibration, the majority of angles within the valid range of the robot arms can be covered by the exoskeleton. Given that the workspaces of most tasks fall within this coverage range, we can teleoperate the robot using the exoskeleton conveniently and intuitively. If a special task t needs a wider operation range, we can simply scale the

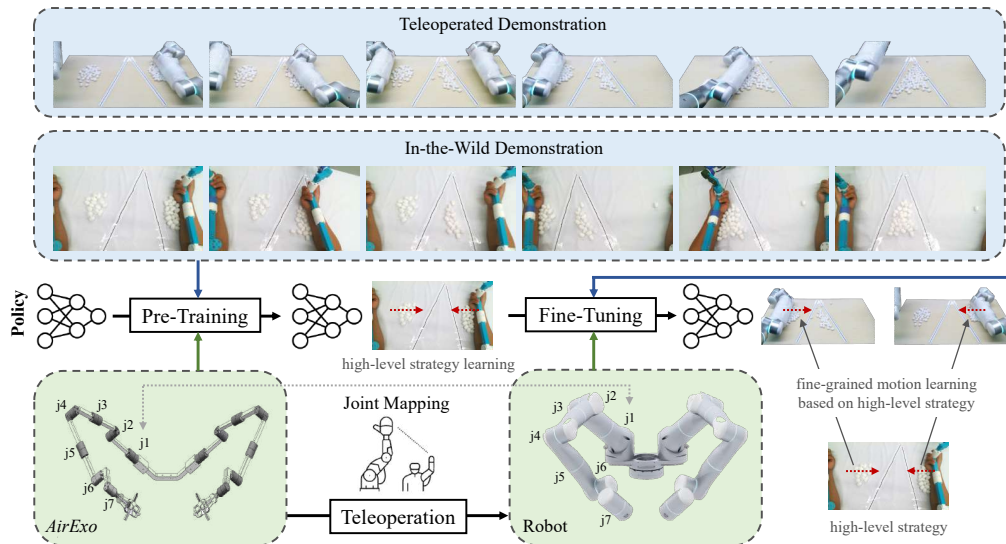


Fig. 3: Overview of learning whole-arm manipulations in the wild with *AirExo*. First, we use in-the-wild demonstrations and exoskeleton actions that are transformed into the robot’s domain to pre-train the policy, which corresponds to learning the high-level strategy of task execution. Then, we use teleoperated demonstrations and robot actions to fine-tune the policy, which corresponds to learning fine-grained motion based on the learned high-level strategy.

exoskeleton range using coefficients k_i , and apply task-specific joint constraint $[q_i^{l,\min}, q_i^{l,\max}]$ instead of original kinematic constraint in Eqn. (1) for better performance.

C. In-the-Wild Learning with *AirExo*

For in-the-wild whole-arm manipulation learning, we install a camera (or cameras under multi-camera settings) on the camera mount of *AirExo* in roughly the same position(s) as the camera(s) on the robot. Using this configuration, images from both teleoperated demonstrations and in-the-wild demonstrations exhibit a relatively similar structure, which is advantageous for policy learning.

Our approach to learn whole-arm manipulation in the wild with *AirExo* is illustrated in Fig. 3. As we discussed in Sec. II-C, *AirExo* serves as a natural bridge for the kinematic gap between humans and robots. To address the domain gap between images, our approach involves a two-stage training process. In the first stage, we pre-train the policy using in-the-wild human demonstrations and actions recorded by the exoskeleton encoders. During this phase, the policy primarily learns the high-level task execution strategy from the large-scale and diverse in-the-wild human demonstrations. Subsequently, in the second stage, the policy undergoes fine-tuning using teleoperated demonstrations with robot actions to refine the motions based on the previously acquired high-level task execution strategy.

As previously discussed in Section III-A, we resize the exoskeleton to ensure its wearability. Some concerns may arise regarding whether this scaling adjustment could impact the policy learning process. Here, we argue that it has a minimal effect on our learning procedure. Firstly, the core kinematic structure, essential for our learning framework, remain unaffected by the resizing. Thus human demonstrations preserve the fundamental dynamics of the system. Secondly, our approach does not impose strict alignment requirements

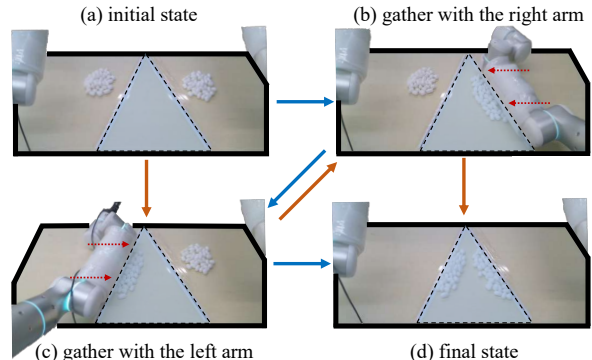


Fig. 4: Definition of *Gather Balls* task. The goal is to gather the balls into the central triangular area, which is highlighted in light blue. The red dashed arrows denote the motions of the robot arms. We use sponge padding to envelop the external surface of the robot arms to diminish the mechanical failures arising from contacts. Note the action multimodality allows accomplishing the task either along the blue arrow or the orange arrow.

between human demonstration images and robot images. We find that similar visual-action pairs collected by our exoskeleton effectively support the pretraining stage, without demanding precise visual matching between human and robot demonstrations.

We use the state-of-the-art bimanual imitation learning method ACT [45] for policy learning. Our experiments demonstrate that it can indeed learn the high-level strategy through the pre-training process and significantly enhance the evaluation performance of the robot and the sample efficiency of the expensive teleoperated demonstrations.

IV. EXPERIMENTS

In this section, we conduct experiments on 2 whole-arm tasks to evaluate the performance of the proposed learning method. All demonstration data are collected by *AirExo*.

# Demos		Method	Completion Rate c (%) \uparrow			Success Rate (%) \uparrow			Collision Rate (%) \downarrow
Teleoperated	In-the-Wild		Overall	Left	Right	$c \geq 80$	$c \geq 60$	$c \geq 40$	
50	-	VIP [21] + NN	27.74	0.02	55.45	0	0	36	0
50	-	VC-1 [22] + NN	52.54	32.53	72.55	4	42	74	0
50	-	MVP [28] + NN	55.10	58.55	62.00	12	62	76	0
50	-	VINN [25]	76.88	75.73	78.03	58	84	94	0
50	-	ConvMLP [43]	15.56	2.35	28.78	0	0	2	4
50	-	BeT [30]	24.66	7.38	41.95	0	2	32	22
50	-	ACT [45]	75.61	94.63	56.60	54	70	100	0
10	-	VINN [25]	68.68	60.28	77.08	36	76	88	0
10	-	ACT [45]	64.31	91.95	36.68	24	60	96	0
10	50	ACT [45]	73.76	88.83	58.70	62	72	88	0
10	100	ACT [45]	75.15	75.63	74.68	56	80	88	0

TABLE I: Experimental results on the *Gather Balls* task.

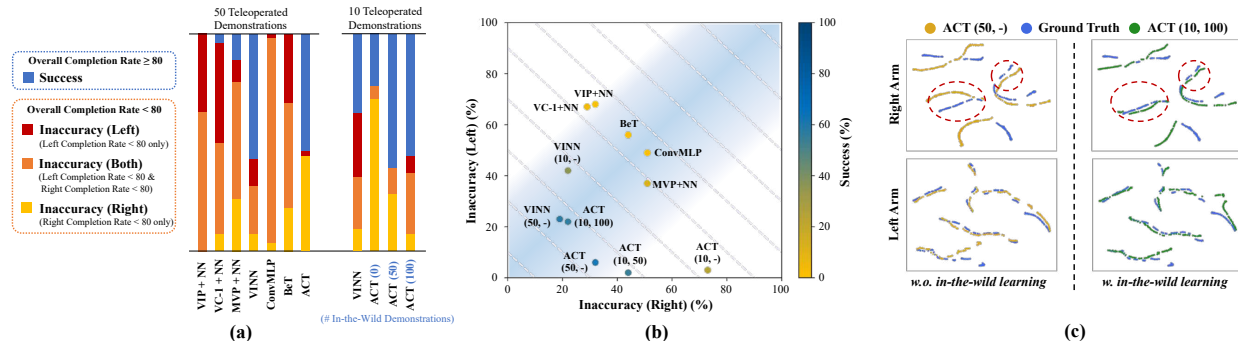


Fig. 5: Analyses of methods on the *Gather Balls* task. Here we define the overall completion rate over 80% as success. (a) We analyze the failure causes of each method in every trial. (b) We amortize the inaccuracy (both) rate evenly into the inaccuracy (left) and inaccuracy (right) rates, and draw a comparison plot of failure modes for different methods. (x,y) means the policy is trained with y in-the-wild demonstrations and then x teleoperated demonstrations. The dashed lines represent contour lines with the same success rate, and the regions with light blue background imply a more balanced policy between left and right arms. (c) t -SNE visualizations of the ground-truth actions and the policy actions w/o in-the-wild learning on the validation set.

A. *Gather Balls*: Setup

1) *Task*: Two clusters of cotton balls are randomly placed on both sides of the tabletop (40 balls per cluster). The goal is to gather these balls into the designated central triangular area using both arms. The process of this contact-rich task is illustrated in Fig. 4.

2) *Metrics*: We consider the percentage of balls being allocated within the central triangular area as the task completion rate c (if a ball is precisely on the line, it is considered a half), including both the completion rates of the left arm and the right arm. Simultaneously, task success is defined as the task completion rate exceeding a certain threshold δ . In this experiment, we set $\delta = 40\%, 60\%, 80\%$. We also record the collision rate to gauge the precision of the operations.

3) *Methods*: We employ VINN [25] and its variants that alter the visual representations [21, 22, 28] as non-parametric methods. Other methods include ConvMLP [43], BeT [30] and ACT [45]. All of them are designed for joint-space control or can be easily adapted for joint-space control. We apply our proposed learning approach to ACT for learning from in-the-wild demonstrations. For all methods, we carefully select the hyper-parameters to ensure better performance.

4) *Protocols*: The evaluation is conducted on a workstation equipped with an Intel Core i9-10980XE CPU. The time limit is set as 60 seconds per trial. Given that all methods can operate at approximately 5Hz, resulting in a total of 300

steps for the evaluation, the time constraint proves sufficient for the task. We conduct 50 consecutive trials to ensure stable and accurate results, calculating the aforementioned metrics.

B. *Gather Balls*: Results and Analyses

The experimental results on the *Gather Balls* task are shown in Tab. I. When using 50 teleoperated demonstrations as training data, VINN performs the best among all non-parametric methods, while ACT excels among all parametric methods. Notice that despite BeT performing well in the state-based simulation environments [30], it appears to struggle in real-world environments, causing collisions. This may be due to the absence of an appropriate state extractor to process images and extract states. When using only 10 teleoperated demonstrations for training, the performance of both VINN and ACT degrades inevitably. However, after applying our in-the-wild learning framework, with the assistance of in-the-wild demonstrations, ACT can achieve the same level of performance as 50 teleoperated demonstrations with just 10 teleoperated demonstrations. This demonstrates that our learning framework with in-the-wild demonstrations makes the policy more sample-efficient for teleoperated demonstrations.

We then delve into the experimental results to provide more insights about why and how our learning framework works. When analyzing the failure cases of different methods

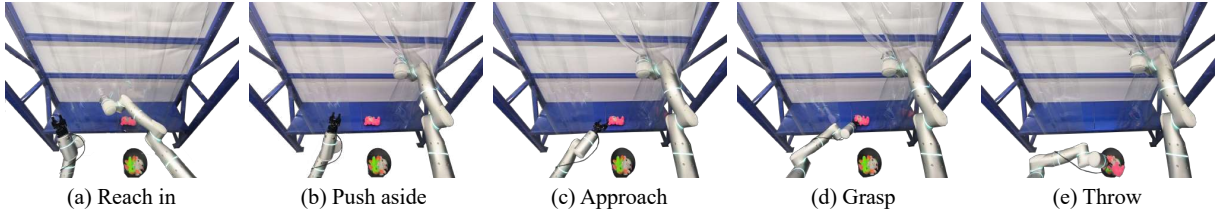


Fig. 6: Definition of the *Grasp from the Curtained Shelf* task. The robot needs to (a) reach in its right arm to the transparent curtain and (b) push aside the curtain, then (c) approach the object with its left arm, (d) grasp the object and finally (e) throw the object.

# Demos		Method	Success Rate (%) \uparrow				
Teleoperated	In-the-Wild		Reach in	Push aside	Approach	Grasp	Throw
50	-	VINN [25]	100	96	92	60	48
50	-	ACT [45]	100	100	100	84	84
10	-	VINN [25]	100	84	84	60	44
10	-	ACT [45]	100	100	96	72	44
10	50	ACT [45]	100	100	96	76	76
10	100	ACT [45]	100	100	100	92	88

TABLE II: Experimental results on the *Grasp from the Curtained Shelf* task.

in the experiments in Fig. 5(a), we find that the ACT policy trained solely on teleoperated demonstrations exhibits an issue of imbalance between accuracies of two arms, with better learning outcomes for the left arm. This imbalance becomes more pronounced as the number of teleoperated demonstrations decreases to 10. With the help of the in-the-wild learning stage, the policy becomes more balanced between two arms even with fewer teleoperated demonstrations, as shown in Fig. 5(b). From Fig. 5(c), we also observe that the policy focuses more on learning the motions of the right arm when cooperated with in-the-wild learning, as highlighted in red dashed circles, while keeping the accurate action predictions on the left arm. We believe that this is attributed to the extensive, diverse, and accurate in-the-wild demonstrations provided by *AirExo*, enabling the policy to acquire high-level strategy knowledge during the pre-training stage. Consequently, in the following fine-tuning stage, it can refine its actions based on the strategy, thus avoiding learning actions blindly from scratch.

C. *Grasp from the Curtained Shelf*: Setup and Results

1) *Task*: A cotton toy is randomly placed in the center of a shelf with curtains. The goal is to grasp the toy and throw it into a bin. To achieve it, the robot needs to use its right arm to push aside the transparent curtain first, and maintain this pose during the following operations. The process of this multi-stage task is illustrated in Fig. 6.

2) *Metrics, Methods, and Protocols*: We calculate the average success rate at the end of each stage as metrics. Based on the experimental results on the *Gather Balls* task, we select VINN [25] and ACT [45] as methods in experiments, as well as ACT equipped with our in-the-wild learning framework. The evaluation protocols are the same as the *Gather Balls* task, except that the time limit is 120 seconds (about 400 steps) and the number of trials is 25.

3) *Results*: The results are given in Tab. II. Similar to the results of the *Gather Balls* task, as the number of training teleoperated demonstrations is reduced, both VINN and ACT

Disturbance	w/o In-the-Wild	Success Rate \uparrow
	Learning	# Success / # Total
Novel Object	\times	4 / 8
	\checkmark	7 / 8
Different Background	\times	2 / 8
	\checkmark	6 / 8
Visual Distractors	\times	4 / 8
	\checkmark	8 / 8

TABLE III: Results of the robustness experiments on the *Grasp from the Curtained Shelf* task.

experience a decrease in success rates, especially in the later “throw” stage. However, after training with our in-the-wild learning framework, ACT exhibits a significant improvement in success rates in the “grasp” and “throw” stages. It achieves even higher success rates, surpassing those obtained with the original set of 50 teleoperated demonstrations lasting more than 20 minutes, using only 10 such demonstrations lasting approximately 3 minutes. This highlights that our proposed in-the-wild framework indeed enables the policy to learn a better strategy, effectively enhancing the success rates in the later stages of multi-stage tasks.

4) *Robustness Analysis*: We design three kinds of disturbances in the robustness experiments to explore whether in-the-wild learning improves the robustness of the policy. The results shown in Tab. III demonstrate that our in-the-wild learning framework can leverage diverse in-the-wild demonstrations to make the learned policy more robust and generalizable to various environmental disturbances.

V. CONCLUSION

In this paper, we develop *AirExo*, an open-source, low-cost, universal, portable, and robust exoskeleton, for both joint-level teleoperation of the dual-arm robot and learning whole-arm manipulations in the wild. Our proposed in-the-wild learning framework decreases the demand for the resource-intensive teleoperated demonstrations. Experimental results show that policies learned through this approach gain a high-level understanding of task execution, leading to improved performance in multi-stage whole-arm manipulation tasks. This outperforms policies trained from scratch using even more teleoperated demonstrations. Furthermore, policies trained in this framework exhibit increased robustness in the presence of various disturbances. In the future, we will investigate how to better address the image gap between in-the-wild data in the human domain and teleoperated data in the robot domain, enabling robots to learn solely through in-the-wild demonstrations with *AirExo*, thus further reducing the learning cost.

VI. ACKNOWLEDGEMENT

We would like to thank Yuanyuan Jia for her help on duplicating *AirExo* to different robotic arms, and Chen Wang at Stanford University for insightful discussion.

Author contributions: H. Fang set up the robot platform, implemented the tele-operation, trained the policy, and wrote the paper. H.-S. Fang initiated the project, devised the experiments, partly designed the exoskeleton, and wrote the paper. Y. Wang designed and implemented the exoskeleton. J. Ren designed and implemented the first version of exoskeleton. J. Chen assisted with data collection and network training. R. Zhang implemented the encoder reading program for the exoskeleton. W. Wang and C. Lu supervised the project and provided hardware and resource support.

REFERENCES

- [1] Shikhar Bahl, Abhinav Gupta, and Deepak Pathak. “Human-to-Robot Imitation in the Wild”. In: *Robotics: Science and Systems (RSS)*. 2022.
- [2] Anthony Brohan et al. “RT-1: Robotics Transformer for Real-World Control at Scale”. In: *Robotics: Science and Systems (RSS)*. 2023.
- [3] Anthony Brohan et al. “RT-2: Vision-Language-Action Models Transfer Web Knowledge to Robotic Control”. In: *arXiv preprint arXiv:2307.15818* (2023).
- [4] Annie S. Chen, Suraj Nair, and Chelsea Finn. “Learning Generalizable Robotic Reward Functions from “In-The-Wild” Human Videos”. In: *Robotics: Science and Systems (RSS)*. 2021.
- [5] Cheng Chi et al. “Diffusion Policy: Visuomotor Policy Learning via Action Diffusion”. In: *Robotics: Science and Systems (RSS)*. 2023.
- [6] Danny Driess et al. “PaLM-E: An Embodied Multimodal Language Model”. In: *International Conference on Machine Learning (ICML)*. Vol. 202. PMLR, 2023, pp. 8469–8488.
- [7] Frederik Ebert et al. “Bridge Data: Boosting Generalization of Robotic Skills with Cross-Domain Datasets”. In: *Robotics: Science and Systems (RSS)*. 2022.
- [8] Fabian Falck, Kawin Larppichet, and Petar Kormushev. “DE VITO: A Dual-Arm, High Degree-of-Freedom, Lightweight, Inexpensive, Passive Upper-Limb Exoskeleton for Robot Teleoperation”. In: *Towards Autonomous Robotic Systems: 20th Annual Conference, TAROS 2019, London, UK, July 3–5, 2019, Proceedings, Part 1 20*. Springer. 2019, pp. 78–89.
- [9] Hao-Shu Fang et al. “AnyGrasp: Robust and Efficient Grasp Perception in Spatial and Temporal Domains”. In: *IEEE Transactions on Robotics (TRO)* (2023).
- [10] Hao-Shu Fang et al. “RH20T: A Robotic Dataset for Learning Diverse Skills in One-Shot”. In: *RSS 2023 Workshop on Learning for Task and Motion Planning*. 2023.
- [11] Flexiv Rizon Robot. URL: <https://www.flexiv.com/en/technology/robot>.
- [12] Franka Emika Panda. URL: <https://www.franka.de/research>.
- [13] Jean-Bastien Grill et al. “Bootstrap Your Own Latent - A New Approach to Self-Supervised Learning”. In: *Advances in Neural Information Processing Systems (NeurIPS)*. Vol. 33. 2020, pp. 21271–21284.
- [14] Yasuhiro Ishiguro et al. “Bilateral Humanoid Teleoperation System Using Whole-Body Exoskeleton Cockpit TABLIS”. In: *IEEE Robotics and Automation Letters* 5.4 (2020), pp. 6419–6426.
- [15] Eric Jang et al. “BC-Z: Zero-Shot Task Generalization with Robotic Imitation Learning”. In: *Conference on Robot Learning (CoRL)*. PMLR. 2021, pp. 991–1002.
- [16] Heecheol Kim, Yoshiyuki Ohmura, and Yasuo Kuniyoshi. “Robot Peels Banana with Goal-Conditioned Dual-Action Deep Imitation Learning”. In: *arXiv preprint arXiv:2203.09749* (2022).
- [17] Heecheol Kim, Yoshiyuki Ohmura, and Yasuo Kuniyoshi. “Transformer-Based Deep Imitation Learning for Dual-Arm Robot Manipulation”. In: *IEEE/RSJ International Conference on Intelligent Robots and Systems (IROS)*. IEEE. 2021, pp. 8965–8972.
- [18] Heecheol Kim et al. “Training Robots Without Robots: Deep Imitation Learning for Master-to-Robot Policy Transfer”. In: *IEEE Robotics and Automation Letters* 8.5 (2023), pp. 2906–2913.
- [19] Kuka IIWA 7R800. URL: <https://www.kuka.com/en-de/products/robot-systems/industrial-robots/lbr-iiwa>.
- [20] Junjia Liu et al. “Robot Cooking with Stir-Fry: Bimanual Non-Prehensile Manipulation of Semi-Fluid Objects”. In: *IEEE Robotics and Automation Letters* 7.2 (2022), pp. 5159–5166.
- [21] Yecheng Jason Ma et al. “VIP: Towards Universal Visual Reward and Representation via Value-Implicit Pre-Training”. In: *International Conference on Learning Representations (ICLR)*. 2023.
- [22] Arjun Majumdar et al. “Where are We in the Search for an Artificial Visual Cortex for Embodied Intelligence?” In: *ICRA 2023 Workshop on Pretraining for Robotics*. 2023.
- [23] Ajay Mandlekar et al. “ROBOTURK: A Crowdsourcing Platform for Robotic Skill Learning through Imitation”. In: *Conference on Robot Learning (CoRL)*. PMLR. 2018, pp. 879–893.
- [24] Suraj Nair et al. “R3M: A Universal Visual Representation for Robot Manipulation”. In: *Conference on Robot Learning (CoRL)*. PMLR. 2022, pp. 892–909.
- [25] Jyothish Pari et al. “The Surprising Effectiveness of Representation Learning for Visual Imitation”. In: *Robotics: Science and Systems (RSS)*. 2022.
- [26] Dean A Pomerleau. “ALVINN: An Autonomous Land Vehicle in a Neural Network”. In: *Advances in Neural Information Processing Systems (NeurIPS)*. Vol. 1. 1988.
- [27] Pragathi Praveena et al. “Characterizing Input Methods for Human-to-Robot Demonstrations”. In: *ACM/IEEE International Conference on Human-Robot Interaction (HRI)*. IEEE. 2019, pp. 344–353.
- [28] Ilija Radosavovic et al. “Real-World Robot Learning with Masked Visual Pre-Training”. In: *Conference on Robot Learning (CoRL)*. PMLR. 2022, pp. 416–426.
- [29] Erick Rosete-Beas et al. “Latent Plans for Task Agnostic Offline Reinforcement Learning”. In: *Conference on Robot Learning (CoRL)*. PMLR. 2022, pp. 1838–1849.
- [30] Nur Muhammad Shafiullah et al. “Behavior Transformers: Cloning k Modes with One Stone”. In: *Advances in Neural Information Processing Systems (NeurIPS)*. Vol. 35. 2022, pp. 22955–22968.
- [31] Anthony Simeonov et al. “Neural Descriptor Fields: SE(3)-Equivariant Object Representations for Manipulation”. In: *IEEE International Conference on Robotics and Automation (ICRA)*. IEEE. 2022, pp. 6394–6400.
- [32] Shuran Song et al. “Grasping in the Wild: Learning 6DoF Closed-Loop Grasping from Low-Cost Demonstrations”. In: *IEEE Robotics and Automation Letters* 5.3 (2020), pp. 4978–4985.
- [33] Kanata Suzuki et al. “In-Air Knotting of Rope Using Dual-Arm Robot Based on Deep Learning”. In: *IEEE/RSJ International Conference on Intelligent Robots and Systems (IROS)*. IEEE. 2021, pp. 6724–6731.
- [34] Alexander Toedtheide et al. “A Force-Sensitive Exoskeleton for Teleoperation: An Application in Elderly Care Robotics”.

- In: *IEEE International Conference on Robotics and Automation (ICRA)*. IEEE. 2023, pp. 12624–12630.
- [35] *UR5 Robot*. URL: <https://www.universal-robots.com/products/ur5-robot>.
 - [36] *ViperX 300 Robot Arm 6DoF*. URL: <https://www.trossenrobotics.com/viperx-300-robot-arm-6dof.aspx>.
 - [37] Chen Wang et al. “MimicPlay: Long-Horizon Imitation Learning by Watching Human Play”. In: *arXiv preprint arXiv:2302.12422* (2023).
 - [38] Thomas Weng et al. “FabricFlowNet: Bimanual Cloth Manipulation with a Flow-based Policy”. In: *Conference on Robot Learning (CoRL)*. PMLR. 2021, pp. 192–202.
 - [39] *WidowX 250 Robot Arm 6DoF*. URL: <https://www.trossenrobotics.com/widowx-250-robot-arm-6dof.aspx>.
 - [40] Fan Xie et al. “Deep Imitation Learning for Bimanual Robotic Manipulation”. In: *Advances in Neural Information Processing Systems (NeurIPS)*. Vol. 33. 2020, pp. 2327–2337.
 - [41] Sarah Young et al. “Visual Imitation Made Easy”. In: *Conference on Robot Learning (CoRL)*. PMLR. 2020, pp. 1992–2005.
 - [42] Andy Zeng et al. “Transporter Networks: Rearranging the Visual World for Robotic Manipulation”. In: *Conference on Robot Learning (CoRL)*. PMLR. 2020, pp. 726–747.
 - [43] Tianhao Zhang et al. “Deep Imitation Learning for Complex Manipulation Tasks from Virtual Reality Teleoperation”. In: *IEEE International Conference on Robotics and Automation (ICRA)*. IEEE. 2018, pp. 5628–5635.
 - [44] Liang Zhao et al. “A Wearable Upper Limb Exoskeleton for Intuitive Teleoperation of Anthropomorphic Manipulators”. In: *Machines* 11.4 (2023), p. 441.
 - [45] Tony Z Zhao et al. “Learning Fine-Grained Bimanual Manipulation with Low-Cost Hardware”. In: *Robotics: Science and Systems (RSS)*. 2023.

APPENDIX

A. AirExo

The key design objective of the exoskeleton system is explained detailedly as follows.

- (1) **Affordability.** The exoskeleton system should be priced at a low level that ensures affordability for a broad spectrum of laboratories and even individual enthusiasts.
- (2) **Adaptability.** The exoskeleton system should be readily adjustable to accommodate various robots without necessitating any modifications the internal joint structure.
- (3) **Portability.** The exoskeleton system should exhibit a lightweight and ergonomic construction, facilitating maneuverability and an extensive array of motions.
- (4) **Robustness.** The exoskeleton system should possess robust durability, enabling it to endure extended operational periods dedicated to demonstration data collection.
- (5) **Maintenance Simplicity.** The components comprising the exoskeleton system should be engineered with an emphasis on simplicity. Assembly ought to be achievable without the requirement of specialized tools, and during maintenance, only a minimal number of components need to be disassembled.

B. Task Parameters

We list the parameters of the tasks in this paper in Tab. IV.

Whole-Arm Manipulation Task	<i>Gather Balls</i>	<i>Grasp from the Curtained Shelf</i>
Hardware Setup (see Appendix D for details)		
# robotic arms	2	2
# cameras	1	2
# gripper	0	1 (left)
Teleoperated Demonstration (TD)		
# TDs	50	50
avg. frequency of the TDs	12.29	6.74
In-the-wild Demonstration (ID)		
# IDs	100	100
avg. frequency of the IDs	13.03	6.65
Evaluation		
# trials	50	25
time limit	60s	120s
Raw Observation		
image dim.	# cameras $\times 3 \times 720 \times 1280$	
depth dim.	# cameras $\times 720 \times 1280$	
joint position dim.	$7 + 7 = 14$	
joint velocity dim.	$7 + 7 = 14$	
tcp position dim.	$7 + 7 = 14$	
tcp velocity dim.	$6 + 6 = 12$	
base force/torque dim.	$6 + 6 = 12$	
tcp force/torque dim.	$6 + 6 = 12$	
gripper dim.	-	6
<i>AirExo</i> encoder dim.	$8 + 8 = 16$	
Reduced Observation and Action		
image dim.	# cameras $\times 3 \times H \times W$	
robot state dim.	$4 + 4 = 8$	$(7 + 1) + 4 = 12$
robot action dim.	$4 + 4 = 8$	$(7 + 1) + 4 = 12$

TABLE IV: Task parameters. Notice that tcp position is represented as (x, y, z) with quaternions (rx, ry, rz, rw) for Flexiv Rizon robotic arms, and gripper information is represented as (width, force, status, width of the last command, force of the last command, timestamp of the last command) for Robotiq 2F-85 grippers.

C. Model Parameters

In this section, we will introduce the detailed implementation of the methods applied in the paper.

Parameters	VIP	VC-1	MVP	VINN
backbone	ResNet-50	ViT-L	ViT-L	ResNet-50
emb. dim.	1024	1024	1024	2048
w/wo pre-trained	✓	✓	✓	
w/wo training	✓			✓
# neighbors	50	10	10	20
action frequency	5Hz	1Hz	1Hz	0.5Hz
control frequency	5Hz	5Hz	5Hz	5Hz

TABLE V: Parameters of Visual Representation Models

The official training code for MVP and VC-1 is not publicly released. Therefore we just use the pre-trained visual representations of these models. For VIP, we fine-tune the pre-trained models in our collected data. For VINN, we use their implementation to train the visual representation models from scratch. The parameters of ConvMLP, BeT and ACT are listed in Tab. VI, Tab. VII and Tab. VIII respectively.

Parameters	<i>Gather Balls</i>
vision backbone	ResNet-50
hidden dim.	1024
batch size	32
learning rate	0.00001
# epochs	1000
action frequency for training	2Hz
control frequency	5Hz

TABLE VI: Parameters of ConvMLP. The 3-layer MLP has a structure of (input dim, hidden dim, output dim).

Parameters	<i>Gather Balls</i>
visual representation type	VINN
number of clusters	32
history horizon	1
GPT block size	144
GPT # layer	6
GPT # head	8
GPT # embd	256
batch size	256
learning rate	0.000001
# epochs	1000
action frequency for training	5Hz
control frequency	5Hz

TABLE VII: Parameters of BeT. We leverage the best-performed visual representations in former experiments (BYOL-trained visual representations used in VINN) to extract the states from images.

Parameters	<i>Gather Balls</i>	<i>Grasp from the Curtained Shelf</i>
hidden dim.	1024	1024
feedforward dim.	6400	6400
KL weight	10	10
chunk size	20	20
batch size for pre-training	64	32
learning rate for pre-training	0.00002	0.00002
# epochs for pre-training	10	10
batch size for fine-tuning	64	32
learning rate for fine-tuning	0.00001	0.00001
# epochs for fine-tuning	1000	1000
action frequency for training	10Hz	5Hz
temporal ensemble k	0.01	0.01
control frequency	5Hz	5Hz

TABLE VIII: Parameters of ACT. Notice that we train all samples of all trajectories in an epoch, instead of sampling one sample of each trajectory in the original ACT implementation [45]. Hence, the number of epochs here is enough for the experiments.

D. Hardware Setup

The hardware setup for teleoperation, in-the-wild demonstration collection and experiments is shown in Fig. 7.

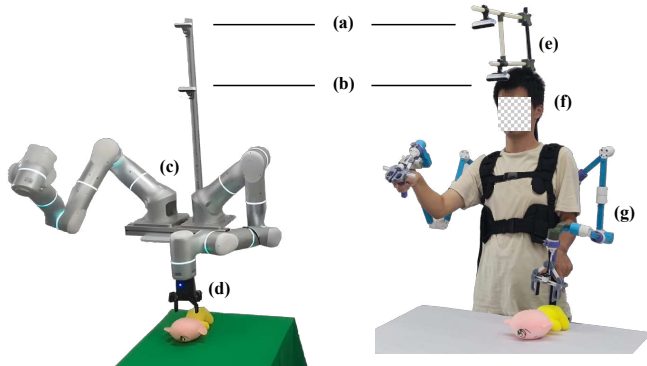


Fig. 7: Hardware setup for teleoperation, in-the-wild demonstration collection and experiments. (a) Intel RealSense D415 RGB-D camera. This camera is only used in the *Grasp from the Curtained Shelf* task. (b) Intel RealSense D415 RGB-D camera. This camera is used in both tasks. (c) Flexiv Rizon dual-arm robots. (d) Robotiq 2F-85 gripper. (e) Adjustable camera mounts. (f) Human operator. (g) Exoskeleton in *AirExo*.

E. Experiments Details

For the *Gather Balls* task, we use the white cotton balls with a diameter of about 2 to 3 centimeters during demonstration collections and experiments. For in-the-wild demonstrations, we also utilize the colored balls of the same size to demonstrate diversity.

For the *Grasp from the Curtained Shelf* task, we use 11 cotton toys (object #9 to #19) during demonstration collections and standard experiments, and 8 cotton toys during robustness experiments (object #1 to #8). We randomly select 10 teleoperated demonstrations out of a total of 50 teleoperated demonstrations in experiments. The objects involved in these 10 demonstrations are shown in Fig. 9(c), and the rest objects are shown in Fig. 9(b). During robustness experiments with novel objects, we investigate the generalization ability of the policy using objects shown in Fig. 9(a). For robustness experiments with different backgrounds, we fix the object to be grasped as the object #14 (*Minion*) and change 8 different backgrounds, as shown in Fig. 10(a). For robustness experiments with visual distractions, we fix the object to be grasped as the object #10 (*pink tiger*), and collect other 7 household objects as distractions, as shown in Fig. 10(b). From the 1st trial to the 7th trial, we introduce

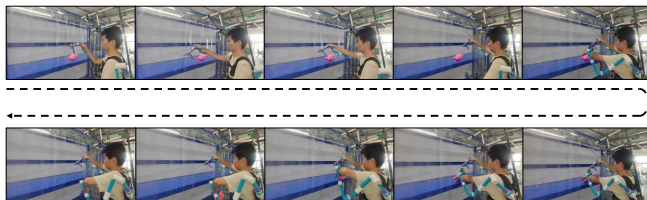


Fig. 8: Sample in-the-wild demonstration process of the *Grasp from the Curtained Shelf* task.

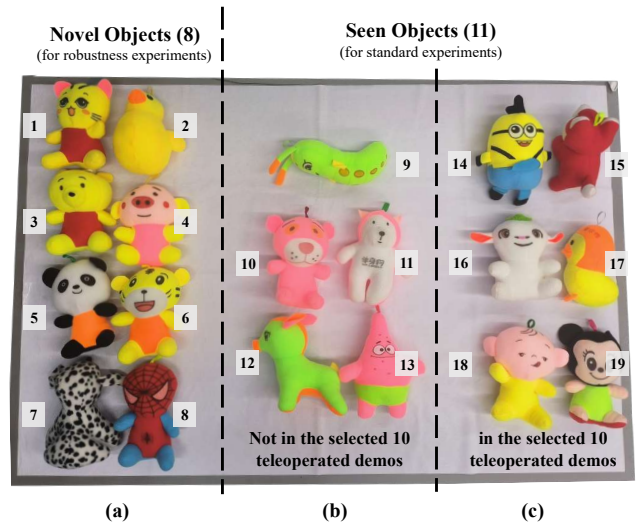


Fig. 9: Objects used in the *Grasp from the Curtained Shelf* task. (a) Novel objects used in robustness experiments, which are not appeared in both teleoperated demonstrations and in-the-wild demonstrations. (b) Seen objects in both demonstrations and experiments, but these objects are not in the selected 10 teleoperated demonstrations in the experiments. (c) Seen objects in both demonstrations and experiments, and these objects are in the selected 10 teleoperated demonstrations. (1: *cat*, 2: *duck*, 3: *yellow bear*, 4: *pig*, 5: *panda*, 6: *yellow tiger*, 7: *dog*, 8: *Spider Man*, 9: *worm*, 10: *pink tiger*, 11: *white bear*, 12: *deer*, 13: *Patrick Star*, 14: *Minion*, 15: *fox*, 16: *Huba*, 17: *chicken*, 18: *baby*, and 19: *Minnie Mouse*)



Fig. 10: Backgrounds and objects used in the *Grasp from the Curtained Shelf* task. (a) 8 different backgrounds used in robustness experiments. (b) 7 visual distractors used in robustness experiments.

one distracting item in each experiment. In the last trial (8th), we place all seven distracting items on the shelf for testing.

F. Demonstration Collection Process and Examples

To collect in-the-wild demonstrations, we place the table or the shelf used in the experiments in front of a human operator, aligning its position relative to the operator with the corresponding position in front of the robot. Then, we adjust the camera position(s) using the adjustable camera mount (Fig. 7(e)) to align with the camera(s) in the robot.

We display the sample in-the-wild data collection process of the *Grasp from the Curtained Shelf* task in Fig. 8.

We also show some examples of teleoperated demonstrations and in-the-wild demonstrations of both tasks (*Gather Balls* and *Grasp from the Curtained Shelf*) in Fig. 11 and Fig. 12 respectively.

For more examples of demonstrations and the data, please refer to our [project website](#).



Fig. 11: Example demonstrations of the *Gather Balls* task.



Fig. 12: Example demonstrations of the *Grasp from the Curtained Shelf* task. Notice that the setting of this task involves two cameras.